^{18}F-FDG PET radiomics for predicting progression-free survival in locally advanced cervical squamous cell carcinoma

Dinghua Pang[1*] MM,
Shilai Zhang[1*] MM,
Hong Yang[1*] MM,
Kaili Liang[2] MM,
Ziya Liu[1] MM,
Zhi Yang[1] PhD,
Chang Yan[3] MM,
Hongjiao Wei[1] BS,
Hai Liao[1] PhD,
Guoyou Xiao[1] BS

**Dinghua Pang, Shilai Zhang, and Hong Yang contributed equally to the writing of this article.*

1. Department of Nuclear Medicine, Guangxi Medical University Cancer Hospital, Nanning 530021, Guangxi Zhuang Autonomous Region, China
2. Department of gynecology, Guangxi Medical University Cancer Hospital, Nanning 530021, Guangxi Zhuang Autonomous Region, China
3. Radiotherapy Center of Guangxi Medical University Cancer Hospital, Nanning 530021, Guangxi Zhuang Autonomous Region, China

Keywords: ^{18}F-FDG PET-Cervical squamous cell carcinoma
- Concurrent chemoradiotherapy
- Progressionfree surviva
- Radiomics

Corresponding author:
Guoyou Xiao,
Department of Nuclear Medicine, Guangxi Medical University Cancer Hospital, No.71 Hedi Road, Qingxiu District, 530021Nanning, Guangxi Zhuang Autonomous Region, China
Tel: +86 13807807280;
xgy725@aliyun.com

Received:
7 October 2025
Accepted revised:
6 December 2025

Abstract

Objective: To develop a fluorine-18-fluorodeoxyglucose (^{18}F-FDG) positron emission tomography (PET) radiomics-based nomogram model for predicting progression-free survival (PFS) in locally advanced cervical squamous cell carcinoma (LACSC) patients undergoing concurrent chemoradiotherapy (CCRT). **Materials and Methods:** A retrospective study included 241 LACSC patients treated with CCRT, divided into training (n=168) and validation (n=73) sets. Lesion segmentation, radiomics feature extraction and screening were performed on ^{18}F-FDG PET images of each patient, and radiomics scores (Rad-scores) were calculated. Univariate and multivariate Cox regression analyses were used to identify independent prognostic factors and create a combined model and nomogram. Predictive performance was assessed using time-dependent receiver operating characteristic (ROC) curves, area under the curve (AUC), and consistency index (C-index). Calibration curves evaluated nomogram accuracy, and decision curve analysis (DCA) assessed nomogram clinical applicability. **Results:** The Rad-score calculated from five optimal radiomics features and FIGO stage were independent predictors of PFS in LACSC patients. The C-index values for the FIGO stage, Rad-score, and combined model were 0.586, 0.692, and 0.727 in the training set, and 0.612, 0.668, and 0.698 in the validation set, respectively. The combined model showed excellent predictive ability for PFS at 12, 18, and 24 months, with training set AUC of 0.805, 0.738, and 0.719, and validation set AUC of 0.670, 0.744, and 0.741, respectively. The calibration curves confirmed a good agreement between predicted and actual progression probabilities, with DCA revealing significant clinical net benefits. **Conclusion:** The ^{18}F-FDG PET radiomics-based nomogram effectively predicted PFS in LACSC patients and could support individualized treatment decisions and accurate prognostic evaluations.

Hell J Nucl Med 2025; 28(3): 232-245 *Epub ahead of print: 15 December 2025* *Published online: 30 December 2025*

Introduction

Cervical cancer, the fourth most common malignancy in women globally [1], is predominantly squamous cell carcinoma (SCC), accounting for 70% of cases [2].The 2018 International Federation of Gynecology and Obstetrics (FIGO) staging system classifies IB3-IVA as locally advanced cervical cancer (LACC), representing over two-thirds of cases, with concurrent chemoradiotherapy (CCRT) as the standard treatment [3, 4]. Through CCRT, although 70%-90% of patients achieving complete remission, about one-third experience recurrence within two years, with a median post-recurrence survival of 10-12 months [5]. Therefore, early identification of high-risk patients for personalized treatment adjustments, such as dose escalation or alternative therapies, is crucial to reduce treatment failure and recurrence.

Previous studies link clinicopathological indicators like histological type, tumor size, and lymph node metastasis to LACC prognosis [6-8]. However, patients with similar clinicopathological features often have divergent clinical outcomes, highlighting the need for more precise prognostic biomarkers to enhance treatment management and patient survival. Given that the current LACC-related treatment relies heavily on imaging evaluations, some scholars suggest using functional imaging parameters for risk stratification and survival rate prediction in cervical cancer patients [9, 10]. Nonetheless, partial studies reported that such indicators are unstable and vary with different quantitative techniques [11, 12].

Radiomics, a promising translational research field, extracts imaging features from medical images and integrates machine learning to correlate high-through put imaging markers with biological data, improving disease interpretation and management [13]. Recently, radiomics-based imaging markers have made significant progress in the auxiliary diagnosis, efficacy evaluation and prognosis prediction of cervical cancer [14-16]. However,

most of the previous studies on the correlation between radiomics and the prognosis of LACC used magnetic resonance imaging (MRI) as the main data source, focusing on the morphological structure, cell density and hemodynamics of the tumor [17-19]. Compared with MRI, fluorine-18-fluorodeoxyglucose (^{18}F-FDG) positron emission tomography/computed tomography (PET/CT) can realize one-stop whole-body scanning and visually display the metabolic activity information of tumor lesions, which is crucial for evaluating the biological characteristics and prognosis of tumors. It has become a recommended examination for evaluating lymph node and distant metastasis in patients with IB3 or higher stage cervical cancer [20].

Herein, we constructed an ^{18}F-FDG PET radiomics-based nomogram model for evaluating locally advanced cervical squamous cell carcinoma (LACSC) patients' progression-free survival (PFS) and verified its predictive performance. We hypothesized that our multidimensional information fusion approach could more accurately facilitate the prognostic prediction of LACSC patients' PFS than traditional single evaluation methods.

Materials and Methods

Participants

This study was approved by institutional Medical Ethics Committee. Patients who underwent ^{18}F-FDG PET/CT examination pre-CCRT at our institution for LACSC between 2018 and 2021 were included in this retrospective analysis. Inclusion criteria: 1) Cervical mass biopsy, pathologically confirmed as SCC; 2) FIGO stage was IB3-IVA; 3) Accept standardized CCRT; 4) No antitumor therapy was received before PET/CT examination. Exclusion criteria: 1) Combined with other malignant tumors; 2) Incomplete clinical data or unclear PET images make it difficult to identify lesions.

A total of 241 LACSC patients were included and randomly divided into a training set (n=168) and a validation set (n=73) in a 7:3 ratio (Figure1). All patients' clinical stages were categorized per the 2018 FIGO staging system [3].

Clinical data collection and processing

The clinical information of patients collected through the hospital electronic medical record and imaging system includes: age, body mass index (BMI), degree of tissue differentiation, hematological indicators measured within 1 week before treatment [squamous cell carcinoma antigen (SCCA), hemoglobin (HGB), albumin (ALB), d-dimer, neutrophil to lymphocyte ratio (NLR), platelet to lymphocyte ratio (PLR), lymphocyte to monocyte ratio (LMR), neutrophil to monocyte ratio (NMR)], baseline PET/CT data [maximum diameter and metabolic parameters of primary tumor, lymph node metastasis (LNM) status and location].

CCRT regimen

Depending on their conditions, all patients received total pelvic external beam radiotherapy or para-aortic extended field radiotherapy (dose range=1.8~2.4Gy/day, for 5 days/week, totaling 50~67.2Gy). High dose rate brachytherapy was then administered (7Gy each time, once/week, totaling

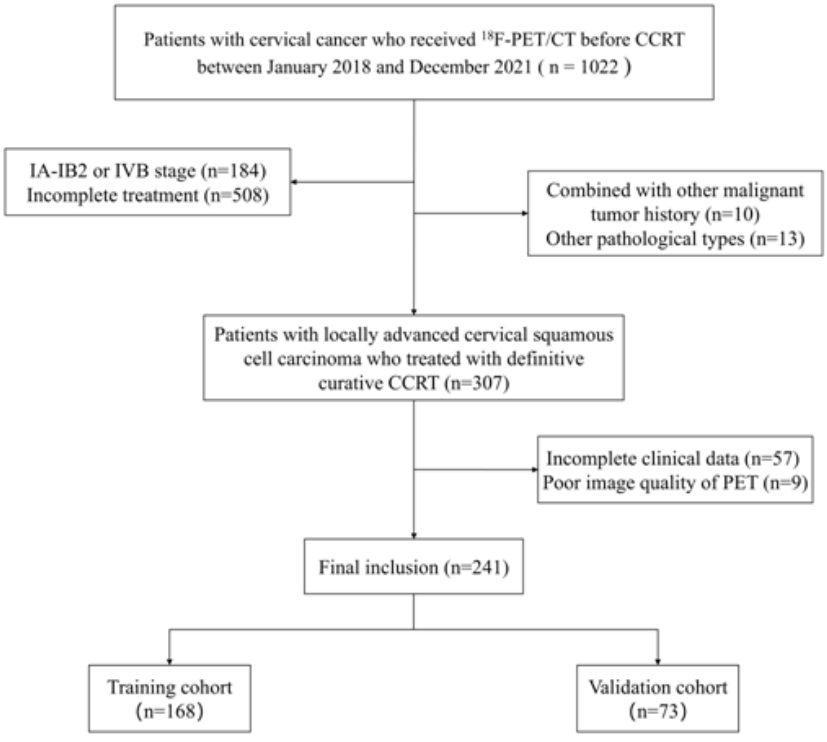

Figure 1. Flow chart of patient selection.

28-42Gy). Meanwhile, all patients received a weekly cisplatin or nedaplatin (50mg/m^2) dose of chemotherapy.

Follow-up program

Regular follow-up was performed post-CCRT, with the first review scheduled in the first month post-CCRT, and then once every 3 months in the first two years, every 6 months in 3-5 years, and every year after 5 years. The review encompassed physical examination, hematological examination, tumor marker detection, imaging examination (B-ultrasound, MRI, CT, and PET/CT), and cervical exfoliative cytology. Herein, PFS was defined as the period from the date of treatment initiation to the date of local recurrence, distant metastasis, death, or last follow-up, whichever came first.

Equipment and imaging

All patients were scanned with GE Discovery 710 PET/CT equipment. The imaging agent ^{18}F-FDG was synthesized in our hospital using a medical cyclotron (HM-10HC) and an ^{18}F-FDG synthesizer system (F300E-2). Radiochemical purity was >95%. All patients were fasted for ≥6h before examination. After controlling the blood glucose concentration to <11.1mmol/L, ^{18}F-FDG (3.70-5.55MBq/kg of body weight) was injected through the elbow vein, with systemic imaging performed 60min post-injection. The scanning area was from the skull top to the middle of the femur. The CT scan parameters were a tube voltage of 120kV, a tube current of 110 mA, and a slice thickness of 3 or 5mm. Notably, PET imaging was performed in a 3D acquisition mode, and 7-8 beds (1.5 min/bed) were collected. After correcting for the non-uniform attenuation in the collected data, the image was fused and reconstructed using the ordered subset maximum expectation algorithm. With a threshold of 40% maximum standardized uptake value (SUV), the primary tumors' SUVmax, SUVmean, SUVpeak, metabolic tumor volume (MTV), and total lesion glycolysis (TLG) in PET/CT images were quantified on the Medex workstation.

Radiomics analysis

Lesion segmentation

First, DICOM format PET images were imported into ITK-SNAP (version 3.8) software [21]. Two seasoned nuclear medicine physicians, each with more than five years of experience, independently outlined the region of interest (ROI) for the primary LACSC lesion. They ensured that the ROI delineated the lesion as much as possible, while excluding necrotic tumor regions and parametrial tissue. To tackle difficulties in determining the lesion's boundaries, they fine-tuned the image contrast and adjusted the axial position. Throughout the delineation process, neither physician had access to the patient's clinical information. To assess delineation consistency, 30 patients were randomly selected, with each physician independently performing lesion ROI delineation.

Feature extraction

PyRadiomics, an open-source tool, was employed to configure image parameters and extract radiomics features, per the Initiative for standardization of imaging biomarkers [22]. All PET images were preprocessed, with the voxel spacing in X, Y, and Z directions resampled to 3mm×3mm×3mm. Absolute intensity resampling and intensity discretization were set to 0~25SUV and 0.25 bin width, respectively. Eight different filtering techniques were used: Laplacian of Gaussian (LOG), wavelet transform, square root, logarithm, exponential, gradient, and three-dimensional local binary patterns (LBP3D), all applied to all patients' images. Seven kinds of features were extracted from both the original and filtered images. They included first order, shape, gray level size zone matrix (GLSZM), gray level run length matrix (GLRLM), neighborhood gray tone difference matrix (NGTDM), gray level co-occurrence matrix (GLCM), and gray level dependence matrix (GLDM).

Feature selection

First, the intraclass correlation coefficient (ICC) was used to test the consistency of the radiomics features extracted from the ROI the two nuclear medicine physicians delineated, and features with ICC >0.75 were retained for subsequent research. Second, all radiomics features were standardized using the Z-score, the Pearson correlation coefficient was used to determine the correlation between radiomics features, and the recursive feature elimination method was used to retain only one feature when the correlation coefficient between any two features exceeded 0.9. Finally, the Least Absolute Shrinkage and Selection Operator (LASSO)-Cox regression and 10-fold cross-validation were used to screen out radiomics features most related to disease progression.

Model construction

Using retained radiomics features and their corresponding co-efficient weighting, we obtained a linear radiomics score (Rad-score) and constructed a radiomics model. The Rad-scores and all clinical parameters were then subjected to univariate and multivariate Cox regression analyses to identify independent prognostic factors for LACSC progression, construct a combined model, and draw a nomogram (Figure 2).

Statistical analysis

Statistical analyses were performed using SPSS (version 26.0), R (version 4.3.1), and Python (version 3.9.7). The Kolmogorov-Smirnov test assessed data normality. Normally distributed data were expressed as mean±SD and compared using the independent sample t-test; non-normally distributed data were expressed as median (IQR) and compared using the Mann-Whitney U test. Count data were expressed as n (%) and compared using the χ^2 test or Fisher's exact test. The Kaplan-Meier method was employed for survival analysis, and the survival rate between groups was compared using the Log-rank test. The COX proportional hazard model with forward stepwise selection was used for multivariate survival analysis to determine the independent prognostic factors of PFS in LACSC patients. The time-dependent receiver operating characteristic (ROC) curve, area under the curve (AUC), and consistency index (C-index) were used to evaluate the model's predictive performance

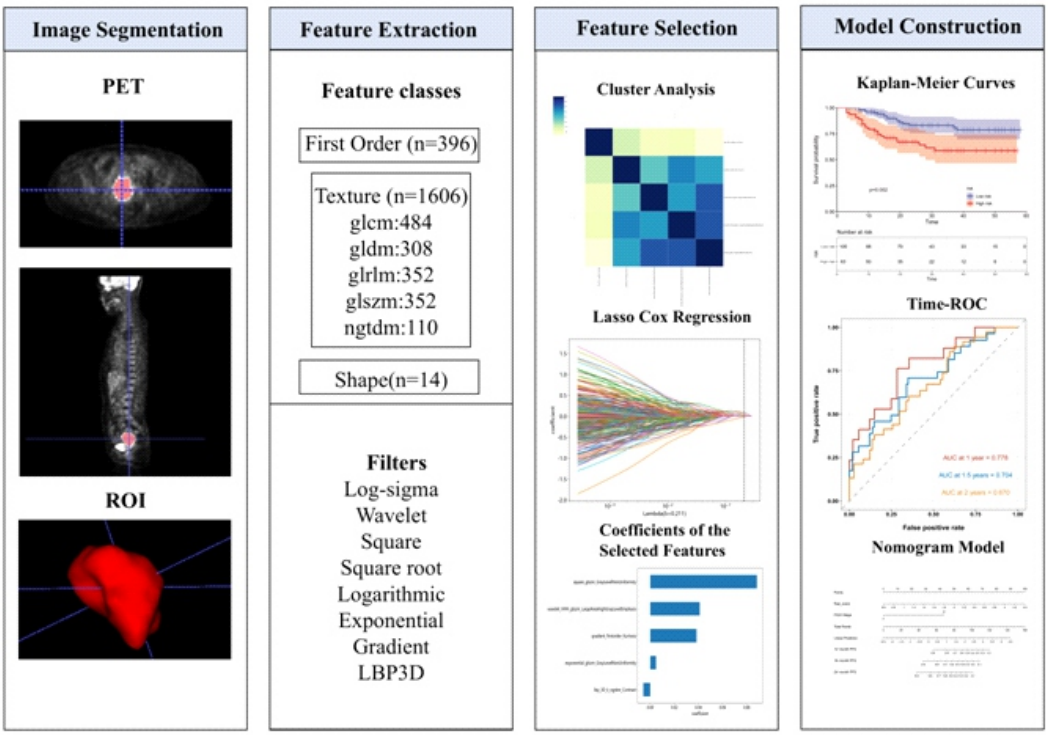

Figure 2. Workflow diagram of radiomics.

for PFS. The R software 'rms' package was used to draw the Nomogram, whose clinical applicability and prediction accuracy were evaluated using decision curve analysis (DCA) and calibration curves, respectively. All statistical tests were two-sided, and results with P<0.05 were considered statistically significant.

Results

Clinical data

The training and validation sets showed no significant difference in clinical indicators (P>0.05). The median follow-up time for all patients was 22.0 months (3-58 months). During follow-up, disease progression was observed in 40 (23.8%) and 21 (28.8%) patients in the training and validation sets, respectively (Table 1).

Screening of radiomics features and Rad-score calculation

We extracted 2,016 radiomics features from ^{18}F-FDG PET images. The average ICC value after the consistency test was 0.978, and a total of 1986 characteristics with ICC ≥0.75 were included in the follow-up study. After Pearson correlation analysis, 371 features with the least redundancy were retained. Finally, after Lasso-Cox regression analysis, 5 PET radiomics features (1 first-order and 4 texture features) most related to PFS were screened out, with a corresponding penalty coefficient λ of 0.211 (Supplementary Figure 1, Supplemental digital content 1). The heat map displays the correlation matrix of radiomics features, illustrating the Pearson correlation coefficient between each feature pair (Supplementary Figure 2, Supplemental digital content 1). The five radiomics features were used to calculate the Rad-score as follows:

$$\begin{aligned}\text{Rad\_score} = {} & -0.005731 \times \text{lbp\_3D\_k\_ngtdm\_Contrast} + 0.004818 \\ & \times \text{exponential\_glszm\_GrayLevelNonUniformity} + 0.038413 \\ & \times \text{gradient\_firstorder\_Kurtosis} + 0.041068 \\ & \times \text{wavelet\_HHH\_glszm\_LargeAreaHighGrayLevelEmphasis} + 0.088484 \\ & \times \text{square\_glszm\_GrayLevelNonUniformity}\end{aligned}$$

Patients were categorized into two groups of different risks of progression based on the optimal critical value of the Rad-score: Low progression risk (Rad-score <1) and high progression risk (Rad-score ≥1). The training set comprised 63 and 105 patients categorized into the high- and low-risk groups, respectively, while the validation set comprised 28 and 45 patients categorized into the high and low-risk groups, respectively. The training and validation sets both exhibited statistically significant differences in FIGO stage, pelvic LNM, tumor size, SUVpeak, MTV, TLG, SCCA, HGB, NLR, PLR and LMR between the high- and low-risk patient groups (P<0.05) (Supplementary Table 1 and Supplementary Table 2, Supplemental digital content 2). Furthermore, the training set showed a significantly lower PFS in the high-risk group than in the low-risk group, with the validation set exhibiting similar results (P<0.05) (Figure 3).

Construction and validation of PFS prediction models

To facilitate the subsequent survival analysis, X-tile software was used to determine the optimal critical value of continuous variables and convert them into a binary from [23]. The

Table 1. *Baseline characteristics of patients in training and validation sets.*

Characteristic	Training set (n=168)	Validation set (n=73)	P value
Age	54.8±9.1	56.4±10.2	0.227
BMI	22.7±3.5	21.9±3.0	0.094
Histological grade			0.348
PD	87 (51.8)	33 (45.2)	
MD+WD	81 (48.2)	40 (54.8)	
FIGO stage			0.828
II	28 (16.7)	13 (17.8)	
III	140 (83.3)	60 (82.2)	
PLNM			0.888
No	72 (42.9)	32 (43.8)	
Yes	96 (57.1)	41 (56.2)	
PALNM			0.332
No	154 (91.7)	64 (87.7)	
Yes	14 (8.3)	9 (12.3)	
Tumor size	4.6 (3.8,6.0)	5.0 (4.3,5.8)	0.279
SUVmax	15.4 (11.5,19.5)	16.6 (13.9,19.6)	0.128
SUVmean	9.1 (6.7,11.7)	9.5 (7.8,12.1)	0.100
SUVpeak	11.6 (8.8,14.1)	12.2 (10.1,14.4)	0.110
MTV	19.4 (10.8,34.5)	24.2 (14.1,37.1)	0.318
TLG	179.6 (89.4,339.4)	240.2 (130.8,371.2)	0.144
SCCA	7.8 (2.9,23.7)	8.5 (3.3,24.7)	0.679
HGB	119.0 (102.0,128.7)	122.0 (111.2,128.0)	0.383
ALB	38.5 (35.5,40.1)	38.1 (35.4,40.2)	0.598
D-dimer	0.28 (0.13,0.52)	0.26 (0.11,0.65)	0.705
NLR	2.3 (1.7,3.5)	2.5 (1.7,4.3)	0.536
PLR	159.0 (121.6,216.7)	151.8 (123.2,217.1)	0.977
LMR	4.3 (3.2,5.7)	4.2 (2.9,5.2)	0.277
NMR	10.6 (8.5,13.0)	9.7 (8.4,12.7)	0.433
Disease progression			0.416
No	128 (76.2)	52 (71.2)	
Yes	40 (23.8)	21 (28.8)	

Note: Variables are presented as mean±SD or median (IQR) for continuous data and n (%) for categorical data. Abbreviation: BMI body mass index, PD poor differentiation, MD middle differentiation, WD well differentiation, FIGO international federation of gynecology and obstetrics, PLNM pelvic lymph node metastasis, PALNM para-aortic lymph node metastasis, SUVmax maximal standardized uptake value, SUVmean mean standard uptake value, SUVpeak Peak standard uptake value, MTV metabolic tumor volume, TLG total lesion glucose, SCCA squamous Cell Carcinoma Antigen, HGB hemoglobin, ALB albumin, NLR neutrophil to lymphocyte ratio, PLR platelet-to-Lymphocyte Ratio, LMR lymphocyte-to-monocyte ratio, NMR Neutrophil to monocyte ratio

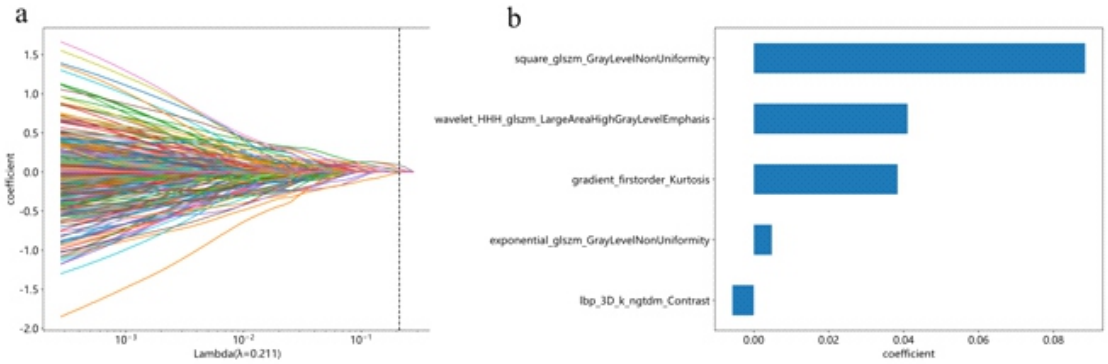

Supplementary Figure 1. Screening of radiomics features. (a) 10-fold cross-validation method was used to select the optimal parameter λ in LASSO-COX regression; (b) The selected radiomics features and their coefficient maps.

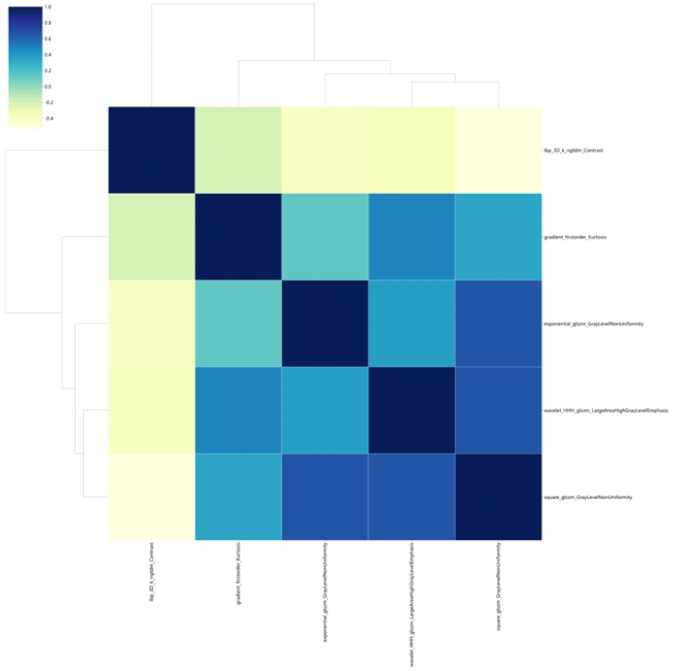

Supplementary Figure 2. Correlation matrix heat map of optimal radiomics features, showing Pearson correlation coefficient between each pair of radiomics features; radiomics features are reordered by unsupervised hierarchical clustering to visualize internal highly correlated features.

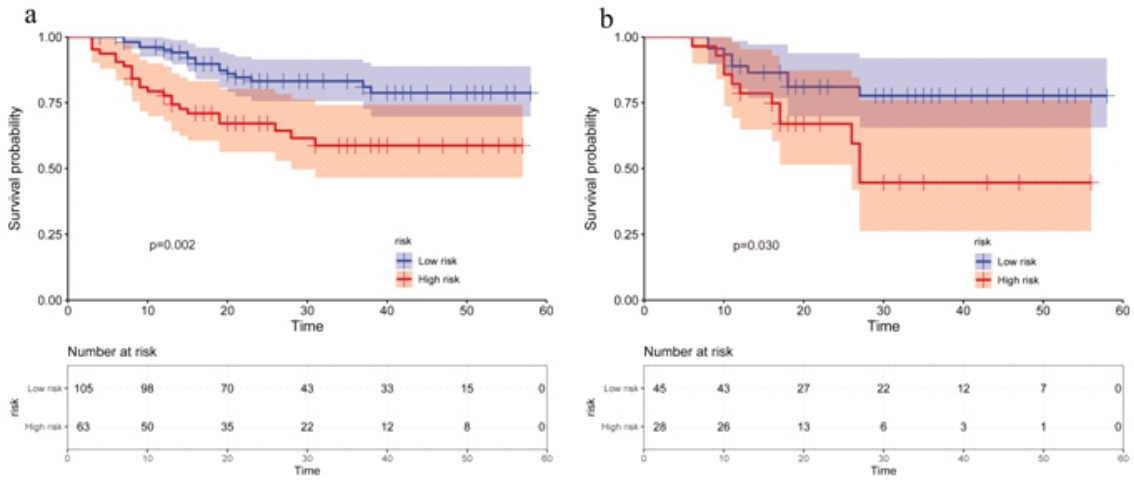

Figure 3. Kaplan-Meier survival curve based on radiomics score in training set (a) and validation set (b).

Supplementary Table 1. *Comparison of clinical characteristics between high-risk and low-risk patients in training set.*

Characteristic	Low-risk group(n=105)	High-risk group (n=63)	P value
Age	55.6±8.5	53.6±10.0	0.170
BMI	22.8±3.3	22.6±3.7	0.785
Histological grade			0.604
PD	56 (53.3)	31 (49.2)	
MD+WD	49 (46.7)	32 (50.8)	
FIGO stage			0.019
II	23 (21.9)	5 (7.9)	
III	82 (78.1)	58 (92.1)	
PLNM			0.024
No	52 (49.5)	20 (31.7)	
Yes	53 (50.5)	43 (68.3)	
PALNM			0.885
No	96 (91.4)	58 (92.1)	
Yes	9 (8.6)	5 (7.9)	
Tumor size	4.6 (3.8,6.0)	5.0 (4.3,5.8)	<0.001
SUVmax	15.4 (11.5,19.5)	16.6 (13.9,19.6)	0.001
SUVmean	9.1 (6.7,11.7)	9.5 (7.8,12.1)	0.001
SUVpeak	11.6 (8.8,14.1)	12.2 (10.1,14.4)	<0.001
MTV	19.4 (10.8,34.5)	24.2 (14.1,37.1)	<0.001
TLG	179.6 (89.4,339.4)	240.2 (130.8,371.2)	<0.001
SCCA	7.8 (2.9,23.7)	8.5 (3.3,24.7)	<0.001
HGB	119.0 (102.0,128.7)	122.0 (111.2,128.0)	<0.001
ALB	38.9 (36.6,40.8)	37.1 (34.3,39.6)	0.001
D-dimer	0.28 (0.13,0.52)	0.26 (0.11,0.65)	0.002
NLR	2.3 (1.7,3.5)	2.5 (1.7,4.3)	<0.001
PLR	159.0 (121.6,216.7)	151.8 (123.2,217.1)	0.001
LMR	4.3 (3.2,5.7)	4.2 (2.9,5.2)	<0.001
NMR	10.6 (8.5,13.0)	9.7 (8.4,12.7)	0.130

Note: Variables are presented as mean±SD or median (IQR) for continuous data and n (%) for categorical data. Abbreviations:BMI body mass index, PD poor differentiation, MD middle differentiation, WD well differentiation, FIGO international federation of gynecology and obstetrics, PLNM pelvic lymph node metastasis, PALNM para-aortic lymph node metastasis, SUVmax maximal standardized uptake value, SUVmean mean standard uptake value, SUVpeak Peak standard uptake value, MTV metabolic tumor volume, TLG total lesion glucose,SCCA squamous cell carcinoma antigen, HGB hemoglobin, ALB albumin, NLR neutrophil to lymphocyte ratio, PLR platelet-to-Lymphocyte Ratio, LMR lymphocyte-to-monocyte ratio, NMR Neutrophil to monocyte ratio

Supplementary Table 2. *Comparison of clinical characteristics between high-risk and low-risk patients in validation set.*

Characteristic	Low-risk group (n=45)	High-risk group (n=28)	P value
Age	58.4±9.2	53.3±11.1	0.039
BMI	22.2±2.8	21.5±3.3	0.331
Histological grade			0.106
PD	17 (37.8)	16 (57.1)	
MD+WD	28 (62.2)	12 (42.9)	
FIGO stage			0.005
II	13 (28.9)	0 (0.0)	
III	32 (71.1)	28 (100.0)	
PLNM			0.002
No	26 (57.8)	6 (21.4)	
Yes	19 (42.2)	22 (78.6)	
PALNM			0.003
No	44 (97.8)	20 (71.4)	
Yes	1 (2.2)	8 (28.6)	
Tumor size	4.5 (3.6,5.0)	6.3 (5.1,7.1)	<0.001
SUVmax	15.0 (12.2,19.6)	16.9 (15.4,20.5)	0.060
SUVmean	9.5 (7.5,12.4)	9.7 (9.1,12.2)	0.279
SUVpeak	11.9 (9.1,14.4)	13.0 (11.7,15.0)	0.038
MTV	15.6 (8.3,24.2)	38.2 (30.2,49.8)	<0.001
TLG	140.8 (71.1,231.8)	388.0 (305.4,494.4)	<0.001
SCCA	6.5 (2.0,13.0)	20.6 (5.7,33.3)	0.004
HGB	125.0 (114.5,129.0)	114.0 (107.3,124.0)	0.002
ALB	38.3 (36.4,40.2)	36.6 (34.9,40.2)	0.210
D-dimer	0.26(0.12,0.56)	0.24 (0.11,0.78)	0.617
NLR	2.1 (1.5,3.4)	3.2 (2.4,4.7)	0.006
PLR	137.1 (115.1,204.8)	181.2 (136.1,244.4)	0.023
LMR	4.4 (3.1,6.1)	3.4 (2.8,4.6)	0.019
NMR	9.6 (8.1,12.0)	10.0 (8.5,14.0)	0.376

Note: Variables are presented as mean±SD or median (IQR) for continuous data and n (%) for categorical data. Abbreviations:BMI body mass index, PD po-or differentiation, MD middle differentiation, WD well differentiation, FIGO international federation of gynecology and obstetrics, PLNM pelvic lymph node metastasis, PALNM para-aortic lymph node metastasis, SUVmax maximal standardized uptake value, SUVmean mean standard uptake value, SUVpeak Pe-ak standard uptake value, MTV metabolic tumor volume, TLG total lesion glucose,SCCA squamous cell carcinoma antigen, HGB hemoglobin, ALB albumin, NLR neutrophil to lymphocyte ratio, PLR platelet-to-Lymphocyte Ratio, LMR lymphocyte-to-monocyte ratio, NMR Neutrophil to monocyte ratio

training set was subjected to Univariate Cox regression analysis, revealing several factors that were significantly associated with PFS, including FIGO stage, SUVmean, TLG, HGB, and Rad-score(P<0.05). These factors were then subjected to Multivariate Cox regression analysis, revealing that FIGO stage and Rad-score were the independent predictors of PFS in LACSC patients(P<0.05) (Table 2), based on which a combined model was constructed.

The C-index values of the FIGO stage, Rad-score, and combined model were 0.586 (0.545-0.627), 0.692 (0.606-0.778), and 0.727 (0.647-0.807) in the training set, and 0.612 (0.559-0.665), 0.668 (0.558-0.778), and 0.698 (0.596-0.800) in the validation set, respectively (Table 3).

The AUCs for FIGO stage in predicting PFS at 12, 18, and 24 months were 0.596, 0.592, and 0.615 in the training set, and 0.614, 0.628, and 0.667 in the validation set. For Rad-score, the AUC were 0.778, 0.704, and 0.670 in the training set, and 0.646, 0.723, and 0.691 in the validation set. The combined model achieved AUC of 0.805, 0.738, and 0.719 in the training set, and 0.670, 0.744, and 0.741 in the validation set (Figure 4).

Table 2. *Univariate and multivariate COX regression analysis of the training set.*

Characteristic	HR (95% CI)	Pvalue	HR (95% CI)	P value
Age (<55 vs ≥55)	0.779 (0.419-1.449)	0.430		
BMI (<24 vs ≥24)	1.041 (0.529-2.048)	0.907		
Histological grade (PD vs MD+WD)	1.503 (0.803-2.814)	0.202		
FIGO stage (II vs III)	10.219 (1.402-74.506)	0.022	7.949 (1.083-58.344)	0.042
PLNM (no vs yes)	1.285 (0.677-2.437)	0.443		
PA LNM (no vs yes)	1.262 (0.449-3.548)	0.659		
Tumor size (<3 vs ≥3)	1.718 (0.414-7.131)	0.456		
SUVmax (<11.8 vs ≥11.8)	1.011 (0.504-2.026)	0.976		
SUVmean (<11.8 vs ≥11.8)	1.998 (1.053-3.793)	0.034		
SUVpeak (<18.1 vs ≥18.1)	1.295 (0.507-3.311)	0.589		
MTV (<10.8 vs ≥10.8)	1.084 (0.515-2.278)	0.832		
TLG (<178.7 vs ≥178.7)	1.984 (1.035-3.800)	0.039		
SCCA (<1.5 vs ≥1.5)	0.931 (0.390-2.221)	0.872		
HGB (<123 vs ≥123)	0.400 (0.195-0.818)	0.012		
ALB (<40.3 vs ≥40.3)	0.760 (0.336-1.719)	0.509		
D--dimer (<0.4 vs ≥0.4)	1.772 (0.940-3.341)	0.077		
NLR (<2.11 vs ≥2.11)	0.978 (0.510-1.875)	0.946		
PLR (<250 vs ≥250)	1.594 (0.705-3.605)	0.263		
LMR (<5.2 vs ≥5.2)	0.753 (0.368-1.540)	0.437		
NMR (<11 vs ≥11)	1.806 (0.951-3.428)	0.071		
Rad-score	5.948 (3.388-10.444)	<0.001	5.269 (2.961-9.378)	<0.001

Note: BMI body mass index, PD poor differentiation, MD middle differentiation, WD well differentiation, FIGO international federation of gynecology and obstetrics, PLNM pelvic lymph node metastasis, PALNM para-aortic lymph node metastasis, SUVmax maximal standardized uptake value, SUVmean mean standard uptake value, SUVpeak Peak standard uptake value, MTV metabolic tumor volume, TLG total lesion glucose,SCCA squamous cell carcinoma antigen, HGB hemoglobin, ALB albumin, NLR neutrophil to lymphocyte ratio, PLR platelet-to-Lymphocyte Ratio, LMR lymphocyte-to-monocyte ratio, NMR Neutrophil to monocyte ratio

Table 3. *Predictive performance of each model for PFS in patients with LACSC C-index (95% CI).*

Model	Training set	Validation set
FIGO stage	0.586 (0.545-0.627)	0.612 (0.559-0.665)
Rad-score	0.692 (0.606-0.778)	0.668 (0.558-0.778)
Combined model	0.727 (0.647-0.807)	0.698 (0.596-0.800)

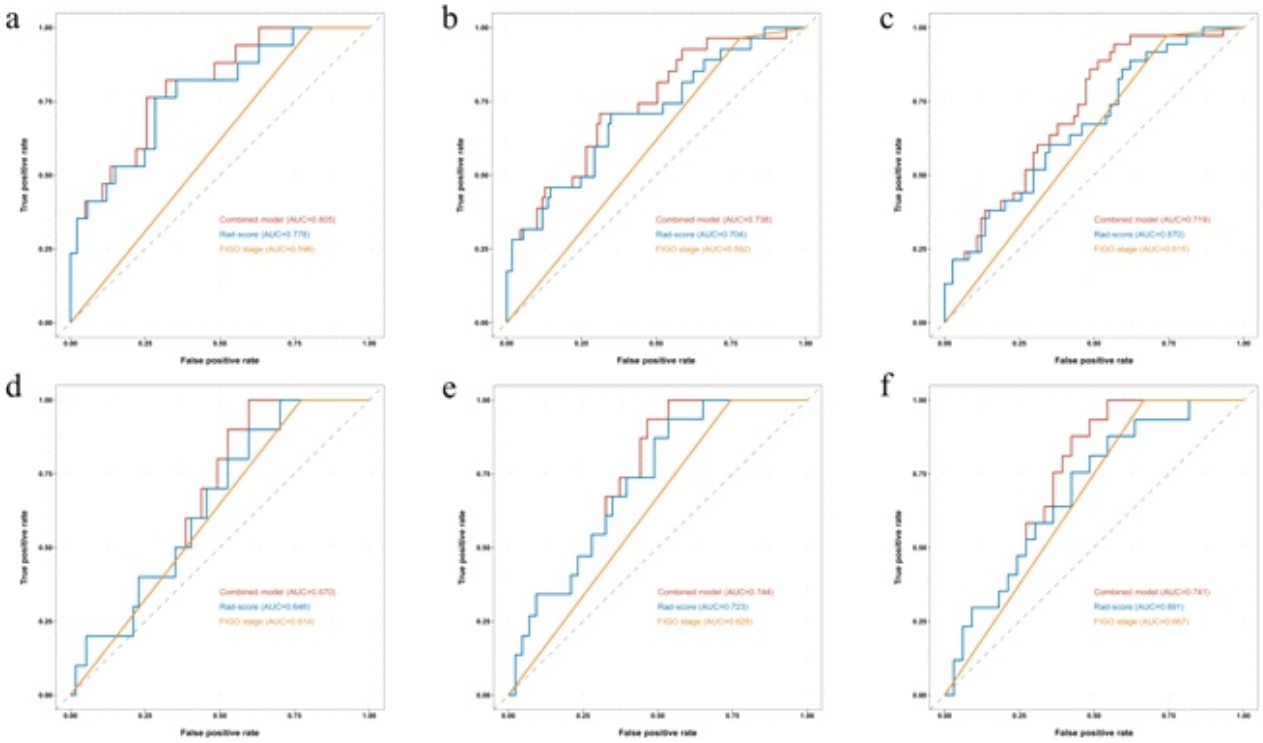

Figure 4. Prediction performance of the three models. (a), (b) and (c) were the ROC curves for predicting PFS of LACSC patients at 12,18 and 24 months in the training set, respectively. (d), (e) and (f) were the ROC curves for predicting PFS of LACSC patients at 12,18 and 24 months in the validation set, respectively.

Nomogram establishment and evaluation

A visual nomogram was built using the Rad-score and FIGO stage (Figure 5). The calibration curve showed that the nomogram model had a good consistency between the predicted and actual probabilities of disease progression (Supplementary Figure 3, Supplemental digital content 1), and the decision curve revealed that the nomogram model could offer more net clinical benefit than the FIGO stage (Supplementary Figure 4, Supplemental digital content 1).

Correlation analysis between Rad-score and PET/CT metabolic parameters

The Rad-scores and PET/CT metabolic parameters of all patients in the study cohort were analyzed using Spearman correlation analysis. According to the results, the Rad-score correlated weakly with SUVmax, SUVmean, and SUVpeak (R= 0.33,0.30,0.41, P<0.001), moderately with MTV (R=0.77, P< 0.001), and strongly with TLG (R=0.81, P<0.001) (Supplementary Figure 5, Supplemental digital content 1).

Discussion

Herein, we developed and validated a pre-CCRT ^{18}F-FDG PET radiomics-based nomogram model for the tailored prediction of PFS in LACSC patients. We found that the baseline ^{18}F-FDG PET radiomics-based model could help physicians stratify patient risk and that the integrated model encompassing the clinical stage not only performed well in predicting the PFS of LACSC patients but also offered more net clinical benefit.

Radiomics can facilitate the diagnosis, efficacy evaluation, and prognostic prediction of cervical cancer [15, 24, 25]. Lucia et al. (2018) [15] found that entropy-GLCMfrom functional imaging DWI-MRI and gray level nonuniformity (GLNU)-GLRL

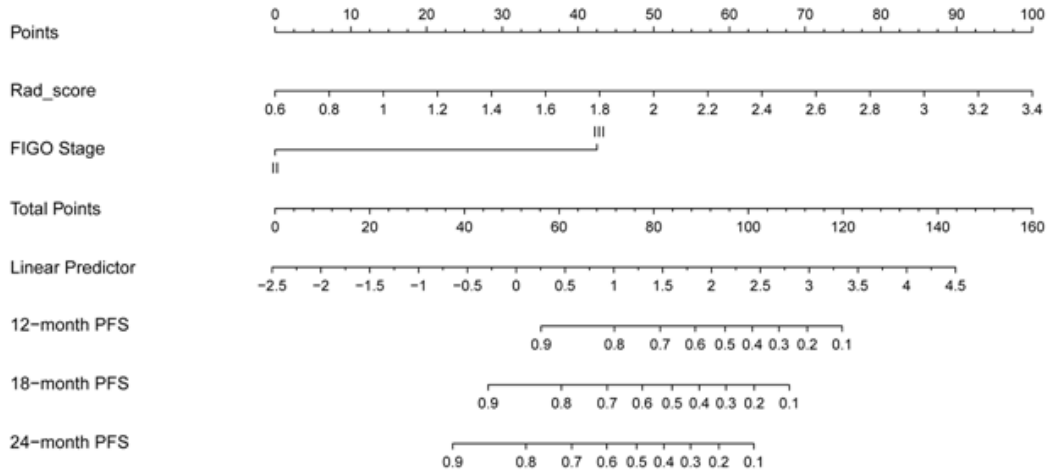

Figure 5. Nomogram model for predicting PFS based on Rad-score and FIGO stage.

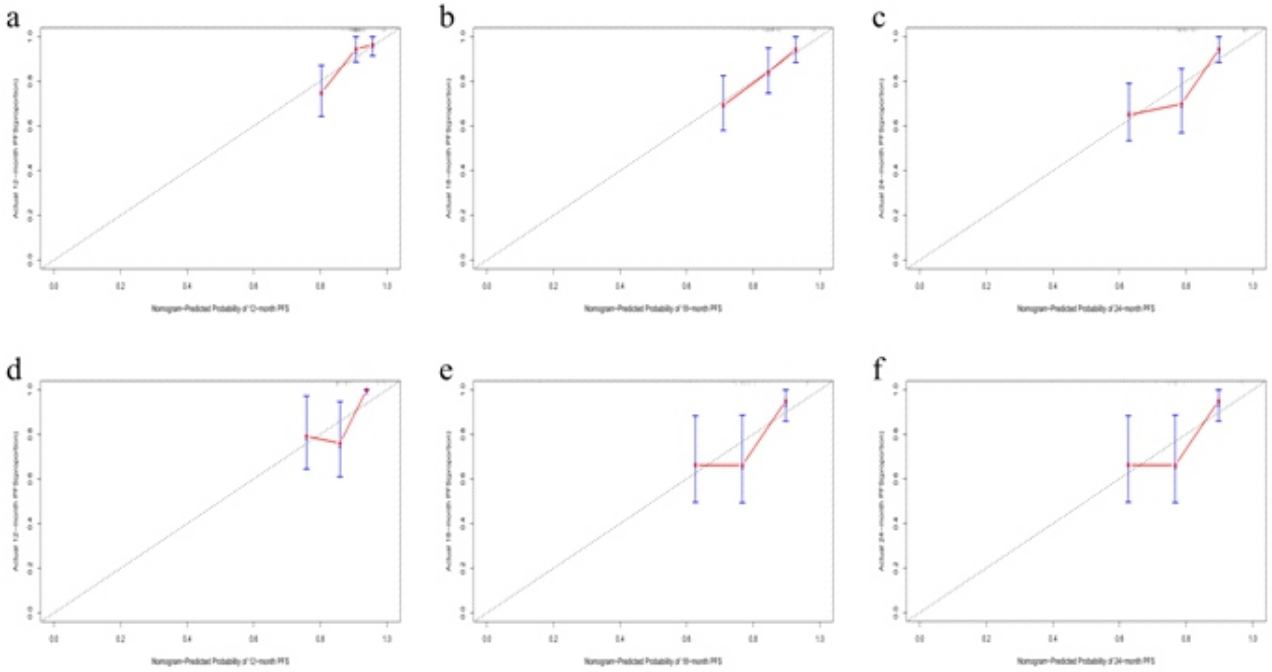

Supplementary Figure 3. (a), (b), and (c) are the nomogram calibration curves of PFS for 12 months, 18 months, and 24 months in the training set, respectively. (d), (e), and (f) are the nomogram calibration curves of PFS for 12 months, 18 months, and 24 months in the validation set, respectively.

from PET were independent predictors of LACC recurrence and local regional control, with a significantly higher predictive capability than that of conventional clinical parameters. Furthermore, Liu et al. (2024) [26] used three CT radiomics features, one PET radiomics feature and one clinical feature to construct a clinical radiomics model for predicting the 3-year PFS of LACC patients post-CCRT, demonstrating good performance. The AUC values of the training, internal test, and external validation sets were 0.661, 0.718 and 0.775, respectively, and the C-index values were 0.698, 0.724 and 0.705, respectively, which align with our findings. Herein, we used a PET radiomics model to predict the PFS of LACSC patients at 12, 18, and 24 months, showing good performance, with validation set AUC values of 0.646, 0.723, and 0.691, respectively. Notably, the combined model integrating the FIGO stage offered more benefits. Among the currently known LACC-related prognostic factors, LNM is a well-documented independent predictor. However, we did not find such a correlation; hence, LNM was not included in our model construction. This phenomenon could be attributed to several factors. Specifi-

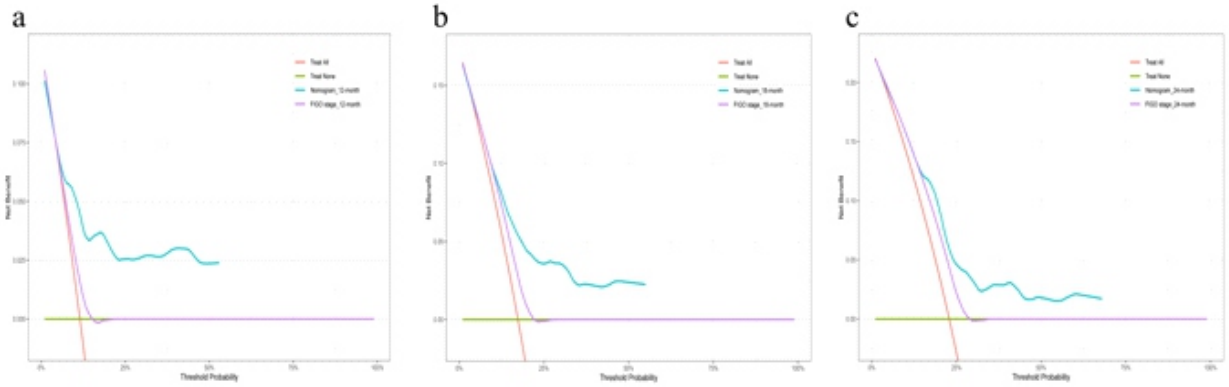

Supplementary Figure 4. (a), (b) and (c) were the decision curve analysis of 12-month, 18-month and 24-month PFS for nomogram model and FIGO staging system, respectively.

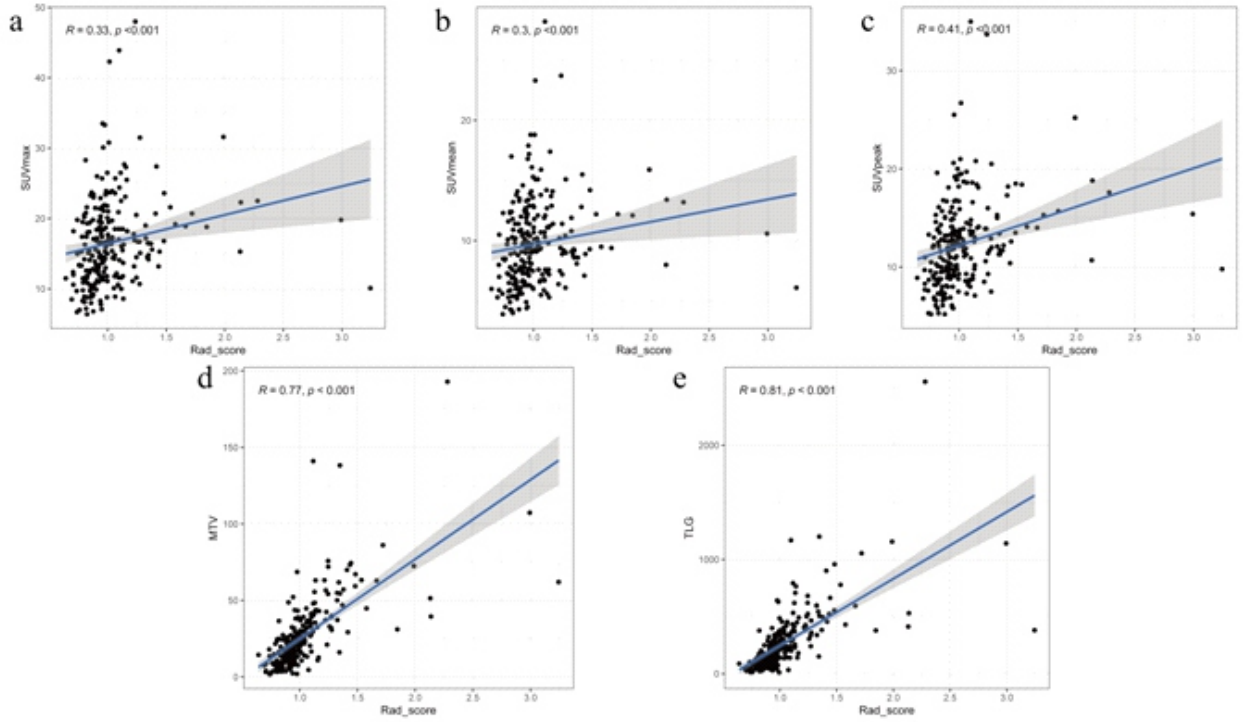

Supplementary Figure 5. Correlation between Rad-score and PET traditional metabolic parameters SUVmax (a), SUVmean (b), SUVpeak (c), MTV (d), TLG (e). The spearman rank correlation test was used to evaluate the relationship between variables.

cally, ^{18}F-FDG PET/CT has moderate sensitivity (72%) and relatively high specificity (96%) in detecting LNM, implying that it could show poor stability when detecting para-aortic LNM [27, 28]. Second, we only considered the location of LNM and not the number of LNM. Olthof et al. (2022) [29] reported that the number of positive lymph nodes could be used to further stratify patient risk in cervical cancer patients. Finally, this study's limited sample size and patient selection bias could also have been influencing factors.

Previously, Kidd et al. (2007) [30] showed that higher SUVmax of cervical cancer primary lesions was associated with poor survival and increased LNM risk. Conversely, we found that SUVmax is not an independent predictor of PFS in LACSC patients, potentially because tumor stage and histological type could affect ^{18}F-FDG uptake in cancer tissues. Furthermore, SUVmax is just a single voxel value that does not reflect the entire tumor's metabolism. Markus et al. (2023) [9] found that only MTV and TLG among the PET/CT metabolic parameters before treatment correlated with recurrence and overall survival in cervical cancer. Moreover, Herrera et al. (2016) [10] and Wang et al. (2021) [31] reported that primary lesion's TLG could be an independent prognostic marker for PFS and distant metastasis-free survival in cervical cancer. Herein, our univariate analysis revealed that both SUVmean and TLG correlated with PFS, although they were not independent predictors in multivariate analysis. Furthermore, the correlation analysis between PET/CT metabolic parameters and Rad-scores showed that SUVmean and

TLG correlated weakly and strongly with Rad-score, respectively. Therefore, our study revealed that compared with traditional metabolic parameters, radiomics features extracted from PET images were more representative and could better identify tumor heterogeneity.

Herein, the PET radiomics model comprised one first-order feature and four texture features. Among them, square_glszm_GrayLevelNonUniformity has the largest weight in our model, indicating that the GLNU from PET images was an important prognostic factor for PFS in cervical cancer patients, which is consistent with previous research [5, 15, 26]. Our results indicate that the uniformity of gray level distribution in PET images correlates closely with the invasiveness of LACSC. Invasive tumor lesions often show uneven gray level distribution on PET images, reflecting significant variations in tumor regions and highlighting blurred, irregular edges. Areas of high metabolic activity absorb more tracers, creating hot spots that intensify with increasing tumor invasiveness. Furthermore, due to the rapid growth and infiltration of highly invasive tumors, there is often no clear boundary between the tumor edge and surrounding normal tissue, manifested as a gradual gray value transition on PET images, rather than a distinct boundary [32, 33]. Highly invasive tumors often induce vascularization to meet their rapidly growing metabolic needs. These new blood vessels may appear as additional hot spots on PET images, further aggravating the uneven distribution of gray levels.

The occurrence and development of tumors often involve changes in the body's immune status, increased inflammatory response, and abnormal activation of the coagulation system [34, 35]. Research has shown that blood metabolites or inflammatory biomarkers are vital predictors of prognosis in cervical cancer patients [36, 37]. However, in this study, inflammatory biomarkers are not independent factors affecting the prognosis of cervical cancer, which may be related to their non-specificity. Some scholars believe that anemia may lead to tumor hypoxia, thereby promoting tumor radioresistance [38]. Chen et al. (2015) [39] found that a low HGB level before treatment correlated with poor local control in LACC patients. Additionally, Liu et al. (2022) [40] found that low HGB levels before CCRT were an independent risk factor for PFS in LACC patients. Herein, our univariate analysis results showed that the HGB level before treatment correlated with the PFS of LACSC patients, although it was not an independent prognostic factor for LACSC in multivariate analysis. This phenomenon could be attributed to the fact that the inclusion of Rad-score somewhat impacted the outcome. Nonetheless, a previous study revealed that anemia was not an independent predictor of cervical cancer recurrence post-CCRT, whereas anemia during radiotherapy was associated with disease-specific survival [41].

This study had some notable limitations. First, it was a small-sample, single-institution, retrospective study. Second, we only analyzed the short-term prognosis. Finally, the tumor ROI was manually delineated in this study. Although the intra-group consistency test revealed that the extracted radiomics features were highly robust, the process was time-consuming and labor-intensive. Therefore, it is necessary to carry out multi-center, long-term prognosis research and explore automatic segmentation technology in the future to improve the prognosis of patients.

In conclusion, the ^{18}F-FDG PET-based Rad-score can more accurately predict the PFS of LACSC CCRT patients, helping clinicians to further stratify patient risk. Meanwhile, the combined nomogram model encompassing the FIGO stage could facilitate a more accurate and personalized assessment of the prognosis of LACSC patients, thus improving clinical benefits.

The authors declare that they have no conflicts of interest.

Funding

This study was supported by Guangxi Science and Technology Project (Guike AB19110015) and Guangxi Biological Targeted Diagnosis and Treatment Research Key Laboratory Open Project (GXSWBX202203, GXSWBX202204, GXSWBX-202205).

Bibliography

1. Sung H, Ferlay J, Siegel RL et al. Global Cancer Statistics 2020: GLOBOCAN Estimates of Incidence and Mortality Worldwide for 36 Cancers in 185 Countries. *CA Cancer J Clin* 2021; 71: 209-49.
2. Wang M, Huang K, Wong MCS et al. Global Cervical Cancer Incidence by Histological Subtype and Implications for Screening Methods. *J Epidemiol Glob Health* 2024; 14: 94-101.
3. Bhatla N, Berek JS, Cuello Fredes M et al. Revised FIGO staging for carcinoma of the cervix uteri. *Int J Gynaecol Obstet* 2019; 145: 129-35.
4. Koh WJ, Abu-Rustum NR, Bean S et al. Cervical Cancer, Version 3.2019, NCCN Clinical Practice Guidelines in Oncology. *J Natl Compr Canc Netw* 2019; 17: 64-84.
5. Nakajo M, Jinguji M, Tani A et al. Machine learning based evaluation of clinical and pretreatment ^{18}F-FDG-PET/CT radiomic features to predict prognosis of cervical cancer patients. *Abdom Radiol (NY)* 2022; 47: 838-47.
6. Yokoi E, Mabuchi S, Takahashi R et al. Impact of histological subtype on survival in patients with locally advanced cervical cancer that were treated with definitive radiotherapy: adenocarcinoma/ adenosquamous carcinoma versus squamous cell carcinoma. *J Gynecol Oncol* 2017; 28: e19.
7. Mccomas KN, Torgeson AM, Ager BJ et al. The variable impact of positive lymph nodes in cervical cancer: Implications of the new FIGO staging system. *Gynecol Oncol* 2020; 156: 85-92.
8. Matsuo K, Mandelbaum RS, Machida H et al. Association of tumor differentiation grade and survival of women with squamous cell carcinoma of the uterine cervix. *J Gynecol Oncol* 2018; 29: e91.
9. Markus M, Sartor H, Bjurberg M, Trägårdh E. Metabolic parameters of ^{18}F-FDG PET-CT before and after radiotherapy may predict survival and recurrence in cervical cancer. *Acta Oncol* 2023; 62: 180-8.
10. Herrera FG, Breuneval T, Prior JO et al. ^{18}F-FDG-PET/CT metabolic parameters as useful prognostic factors in cervical cancer patients treated with chemo-radiotherapy. *Radiat Oncol* 2016; 11: 43.
11. Zhang Y, Hu Y, Zhao S, Cui C. The Utility of PET/CT Metabolic Parameters Measured Based on Fixed Percentage Threshold of SUVmax and Adaptive Iterative Algorithm in the New Revised FIGO Staging System for Stage III Cervical Cancer. *Front Med (Lausanne)* 2021; 8: 680072.
12. Vojtíšek R, Baxa J, Kovářová P et al. Prediction of treatment response in patients with locally advanced cervical cancer using mid-treatment PET/MRI during concurrent chemoradiotherapy. *Strahlenther Onkol* 2021; 197: 494-504.
13. Lambin P, Leijenaar RTH, Deist TM et al. Radiomics: the bridge between medical imaging and personalized medicine. *Nat Rev Clin Oncol* 2017; 14: 749-62.

14. Huang Q, Deng B, Wang Y et al. Reduced field-of-view DWI-derived clinical-radiomics model for the prediction of stage in cervical cancer. *Insights Imaging* 2023; 14: 18.
15. Lucia F, Visvikis D, Desseroit MC et al. Prediction of outcome using pretreatment ^{18}F-FDG PET/CT and MRI radiomics in locally advanced cervical cancer treated with chemoradiotherapy. *Eur J Nucl Med Mol Imaging* 2018; 45: 768-86.
16. Zhang X, Zhang Q, Chen Y et al. MRI-based radiomics for pretreatment prediction of response to concurrent chemoradiotherapy in locally advanced cervical squamous cell cancer. *Abdom Radiol (NY)* 2023; 48: 367-76.
17. Tang S, Yen A, Wang K et al. Progression-Free Survival Prediction for Locally Advanced Cervical Cancer After Chemoradiotherapy With MRI-based Radiomics. *Clin Oncol (R Coll Radiol)* 2025; 38: 103702.
18. Ikushima H, Haga A, Ando K et al. Prediction of out-of-field recurrence after chemoradiotherapy for cervical cancer using a combination model of clinical parameters and magnetic resonance imaging radiomics: a multi-institutional study of the Japanese Radiation Oncology Study Group. *J Radiat Res* 2022; 63: 98-106.
19. Liu J, Dong L, Zhang X et al. Radiomics analysis for prediction of lymph node metastasis after neoadjuvant chemotherapy based on pretreatment MRI in patients with locally advanced cervical cancer. *Front Oncol* 2024; 14: 1376640.
20. Manganaro L, Lakhman Y, Bharwani N et al. Correction to: Staging, recurrence and follow-up of uterine cervical cancer using MRI: Updated Guidelines of the European Society of Urogenital Radiology after revised FIGO staging 2018. *Eur Radiol* 2022;32:738.
21. Yushkevich PA, Piven J, Hazlett HC et al. User-guided 3D active contour segmentation of anatomical structures: significantly improved efficiency and reliability. *Neuroimage* 2006; 31: 1116-28.
22. Zwanenburg A, Vallières M, Abdalah MA et al. The Image Biomarker Standardization Initiative: Standardized Quantitative Radiomics for High-Throughput Image-based Phenotyping. *Radiology* 2020; 295: 328-38.
23. Camp RL, Dolled-Filhart M, Rimm DL. X-tile: a new bio-informatics tool for biomarker assessment and outcome-based cut-point optimization. *Clin Cancer Res* 2004; 10: 7252-9.
24. Liu Y, Song T, Dong TF et al. MRI-based radiomics analysis to evaluate the clinicopathological characteristics of cervical carcinoma: a multicenter study. *Acta Radiol* 2023; 64: 395-403.
25. Gui B, Autorino R, Miccò M et al. Pretreatment MRI Radiomics Based Response Prediction Model in Locally Advanced Cervical Cancer. *Diagnostics (Basel)* 2021; 11: 631.
26. Liu H, Cui Y, Chang C et al. Development and validation of a ^{18}F-FDG PET/CT radiomics nomogram for predicting progression free survival in locally advanced cervical cancer: a retrospective multicenter study. *BMC Cancer* 2024; 24: 150.
27. Ruan J, Zhang Y, Ren H. Meta-analysis of PET/CT Detect Lymph Nodes Metastases of Cervical Cancer. *Open Med (Wars)* 2018; 13: 436-42.
28. Martinez A, Voglimacci M, Lusque A et al. Tumour and pelvic lymph node metabolic activity on ^{18}FDG-PET/CT to stratify patients for para-aortic surgical staging in locally advanced cervical cancer. *Eur J Nucl Med Mol Imaging* 2020; 47: 1252-60.
29. Olthof EP, Mom CH, Snijders MLH et al. The prognostic value of the number of positive lymph nodes and the lymph node ratio in early-stage cervical cancer. *Acta Obstet Gynecol Scand* 2022; 101: 550-7.
30. Kidd EA, Siegel BA, Dehdashti F, Grigsby PW. The standardized uptake value for F-18 fluorodeoxyglucose is a sensitive predictive biomarker for cervical cancer treatment response and survival. *Cancer* 2007; 110: 1738-44.
31. Wang D, Liu X, Wang W et al. The Role of the Metabolic Parameters of ^{18}F-FDG PET/CT in Patients With Locally Advanced Cervical Cancer. *Front Oncol* 2021; 11: 698744.
32. Yin Q, Hung SC, Wang L et al. Associations between Tumor Vascularity, Vascular Endothelial Growth Factor Expression and PET/MRI Radiomic Signatures in Primary Clear-Cell-Renal-Cell-Carcinoma: Proof-of-Concept Study. *Sci Rep* 2017; 7: 43356.
33. Mazzara S, Travaini L, Botta F et al. Gene expression profiling and ^{18}FDG-PET radiomics uncover radiometabolic signatures associated with outcome in DLBCL. *Blood Adv* 2023; 7: 630-43.
34. Rubio-Jurado B, Balderas-Peña LM, García-Luna EE et al. Obesity, Thrombotic Risk, and Inflammation in Cancer. *Adv Clin Chem* 2018; 85: 71-89.
35. Moik F, Ay C. Hemostasis and cancer: Impact of haemostatic biomarkers for the prediction of clinical outcomes in patients with cancer. *J Thromb Haemost* 2022; 20: 2733-45.
36. Elmali A, Guler OC, Demirhan B et al. Long-term analysis of hematological parameters as predictors of recurrence patterns and treatment outcomes in cervical cancer patients undergoing definitive chemoradiotherapy. *Strahlenther Onkol* 2024; 200: 949-57.
37. Medici F, Ferioli M, Forlani L et al. Decoding the Complexity of Systemic Inflammation Predictors in Locally Advanced Cervical Cancer, with Hemoglobin as the Hidden Key (the ESTHER Study). *Cancers (Basel)* 2023; 15: 5056.
38. Grimes DR, Partridge M. A mechanistic investigation of the oxygen fixation hypothesis and oxygen enhancement ratio. B*iomed Phys Eng Express* 2015; 1: 045209.
39. Chen CC, Wang L, Lin JC, Jan JS. The prognostic factors for locally advanced cervical cancer patients treated by intensity-modulated radiation therapy with concurrent chemotherapy. *J Formos Med Assoc* 2015; 114: 231-7.
40. Liu J, Tang G, Zhou Q, Kuang W. Outcomes and prognostic factors in patients with locally advanced cervical cancer treated with concurrent chemoradiotherapy. *Radiat Oncol* 2022; 17: 142.
41. Bishop AJ, Allen PK, Klopp AHet al. Relationship between low hemoglobin levels and outcomes after treatment with radiation or chemoradiation in patients with cervical cancer: has the impact of anemia been overstated? *Int J Radiat Oncol Biol Phys* 2015; 91: 196-205.